Journal of Non-Crystalline Solids 582 (2022) 121442

Contents lists available at ScienceDirect

Journal of Non-Crystalline Solids

journal homepage: www.elsevier.com/locate/jnoncrysol

# Multiphonon trap ionization mechanism in amorphous $SiN_x$

Yu.N. Novikov [a,*], V.A. Gritsenko [a,b,c]

[a] Rzhanov Institute of Semiconductor Physics SBRAS, 13 Lavrentiev aven., 630090, Novosibirsk, Russia
[b] Novosibirsk National Research University, 2 Pirogov str., 630090, Novosibirsk, Russia
[c] Novosibirsk State Technical University, 20 Marx aven., 630073, Novosibirsk, Russia

ARTICLE INFO

*Keywords:*
amorphous silicon nitride
$SiN_x$
traps
charge transport
multiphonon ionization mechanism

ABSTRACT

The charge transport mechanism in amorphous silicon nitride (a-$SiN_x$) is experimentally analyzed in a wide range of electric fields and temperatures. The Frenkel effect with thermally assisted tunneling (TAT) and the multiphonon mechanism were used to describe the trap ionization. It is shown that the widespread Frenkel effect with TAT formally describes the experiment, but the agreement with the experiment is obtained if a small frequency factor ($10^9$ $s^{-1}$) and a large tunneling effective mass ($m^*$=3$m_0$) are used. Thus, the Frenkel effect does not describe the charge transport in a-$SiN_x$. The charge transport in a-$SiN_x$ is satisfactorily described by the multiphonon trap ionization mechanism with the following parameters: $m^* = 0.6m_0$, thermal and optical energies - $W_T = 1.6$ eV and $W_{OPT} = 3.2$ eV, respectively.

## 1. Introduction

By its definition, a dielectric, unlike a metal and a semiconductor, must not conduct electric current. Currently, dielectric films with a thickness of 3 - 10 nm are widely used in silicon devices. The voltage of 3 V applied to such dielectric forms the electric field 1 - 3 MV/cm. In such strong electric fields, there is a tunnel injection of electrons (holes) from silicon or a metal into a dielectric [1]. In most dielectrics, the charge transport is accomplished using deep centers (electron and hole traps). Most dielectrics, such as amorphous silicon nitride (a-$SiN_x$) [2–4], BN [5], $Al_2O_3$ [6], $ZrO_2$ [7,8], $Ta_2O_5$ [9–11], $GeO_2$ [12], $HfO_2$ [13] and low-k dielectrics [14] have a high trap concentration ($10^{18}$-$10^{21}$) $cm^{-3}$. a-$SiN_x$ is one of the key dielectrics in semiconductor electronics and is of both scientific [15] and practical interest [16]. It has a high concentration of deep ($\approx$ 1.5 eV) traps with a giant retention time of electrons and holes in a localized state (10 years at 85°C), where the hole trap levels are measured from the valence band top, and the electron trap levels are measured from the conduction band bottom. This is the so-called memory effect in silicon nitride [17]. The memory effect in a-$SiN_x$ is used in modern terabit-scale flash memory devices. In such a memory element, electrons or holes localized on traps in a-$SiN_x$ induce or do not induce an inversion conducting channel in a field-effect transistor, which corresponds to a logical “1” or “0”. The charge storage time in a flash memory cell based on silicon nitride depends on the trap energy spectrum in a-$SiN_x$. There are contradictory data on the trap spectrum in a-$SiN_x$ in the literature. Thus, in [2], the electron and hole traps, which are described using a discrete monoenergetic level for electrons and holes, are discussed. At the same time, the continuous spectrum of electron traps in a-$SiN_x$ in the range 0.6–1.8 eV is considered in [18–20]. In [21], a continuous spectrum of electron and hole traps in a-$SiN_x$ was reported in the range of 1.6–2.6 eV and 2.0–2.8 eV, respectively.

Experiments show that, in strong electric fields, the leakage current in a dielectric is increased exponentially with the increasing electric field. In 1938, Frenkel proposed a simple visual model, where the Coulomb trap ionization probability exponentially increases proportionally to the square root of the electric field value.

At present, it is generally accepted that the trap ionization in a-$SiN_x$ is described by the Frenkel effect [2–4,24,25]. The trap ionization in semiconductors, as a rule, is interpreted within the multiphonon ionization theory [26–28]. Recently, the exact quantum theory of multiphonon trap ionization has been used to describe the charge transport in various dielectrics: BN [5], $Al_2O_3$ [6], $Ta_2O_5$ [11], $HfO_2$ [13,29] and low-k dielectrics [14]. In [26], the Bessel functions are used in the formula to describe the multiphonon ionization process. In [28], a simple analytical formula for the multiphonon trap ionization was proposed for high electric fields.

The aim of this work is to experimentally study the charge transport mechanism in a-$SiN_x$ in wide temperature (130 - 600 K) and electric field (2 - 7 MV/cm) ranges, respectively, and compare the experiment with

* Corresponding author:
*E-mail address:* nov@isp.nsc.ru (Yu.N. Novikov).

https://doi.org/10.1016/j.jnoncrysol.2022.121442
Received 18 November 2021; Received in revised form 19 January 2022; Accepted 21 January 2022
0022-3093/© 2022 Elsevier B.V. All rights reserved.

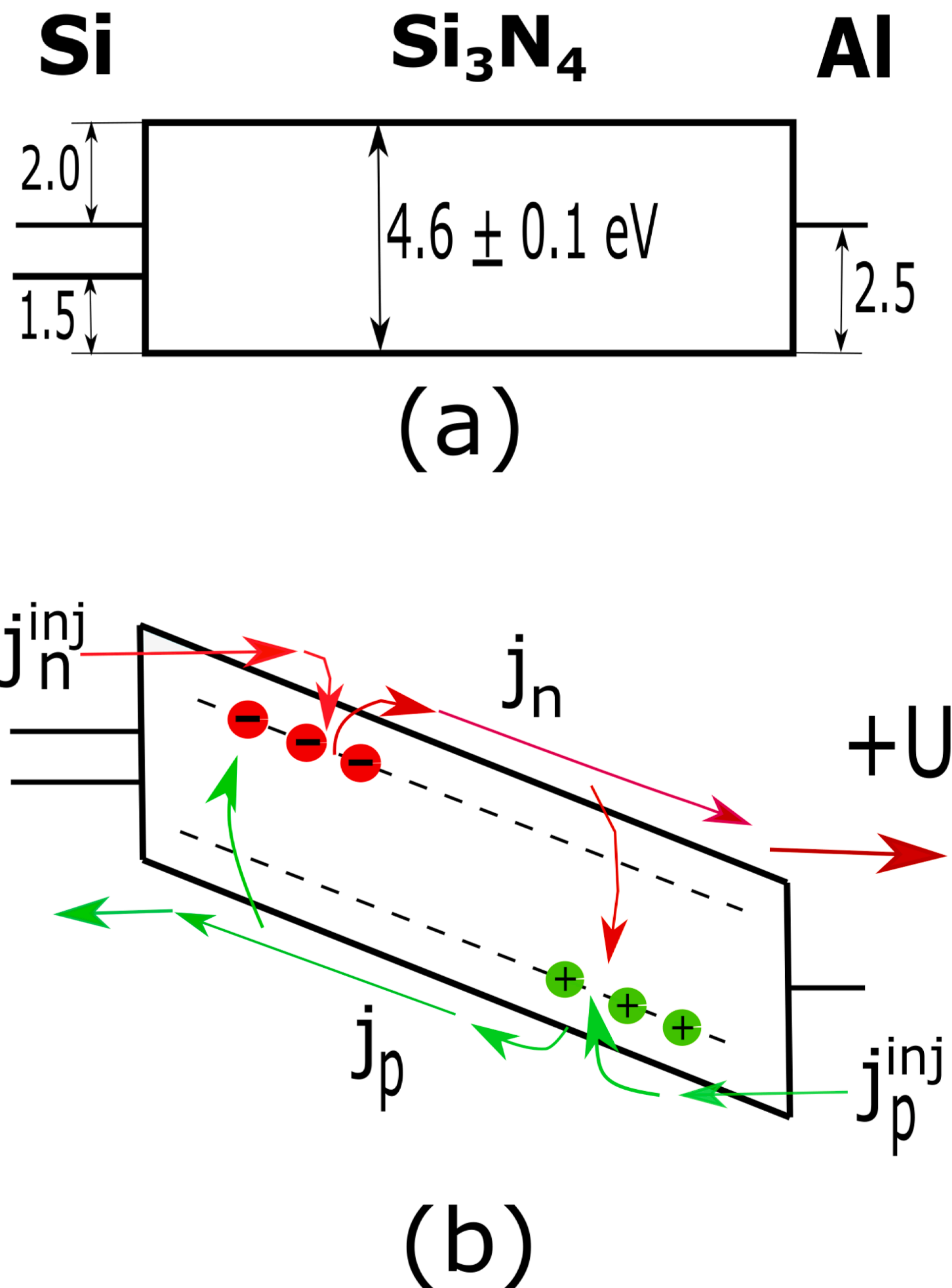


**Fig. 1.** Energy diagram of Si/a-$SiN_x$/Al structure: (a) without applied electric field (b) with a positive potential on Al. The current of electrons and holes is shown with arrows; the dashed lines are the energy levels of electron and hole traps.

the calculation taking into account the two-band conductivity model. To describe the trap ionization probability, two theories were used: the Frenkel effect, along with the thermally assisted tunneling (TAT), and the multiphonon trap ionization theory [26,28].

## 2. Samples, experimental method and calculation

a-$SiN_x$ ($d$ = 92 nm thick) was grown on an n-Si substrate by the pyrolysis of silane-and-ammonia mixture at ratio 1:20 in a hydrogen flow at $850^0$ C. An aluminum metal contact with the area of $5 \times 10^{-3}$ $cm^2$ was deposited onto a-$SiN_x$ through a mask. The temperature dependences of current in Si/a-$SiN_x$/Al structures (at a fixed potential on the Al electrode) were measured in a cryostat in the temperature range 130 – 600 K. The rate of temperature change was ~ 20 K/min.

The energy diagram of the Si/a-$SiN_x$/Al structure is shown in Fig. 1: (a) without applied voltage [30] and (b) with a positive potential on Al. The electron and hole components of the currents are marked with arrows in Fig. 1.

To consider the charge transport in a-$SiN_x$, a one-dimensional two-band model was used. The trap recharging was described using the model [4,31] in which we considered the electron and hole transport. The inhomogeneous electric field in a-$SiN_x$ was calculated using the

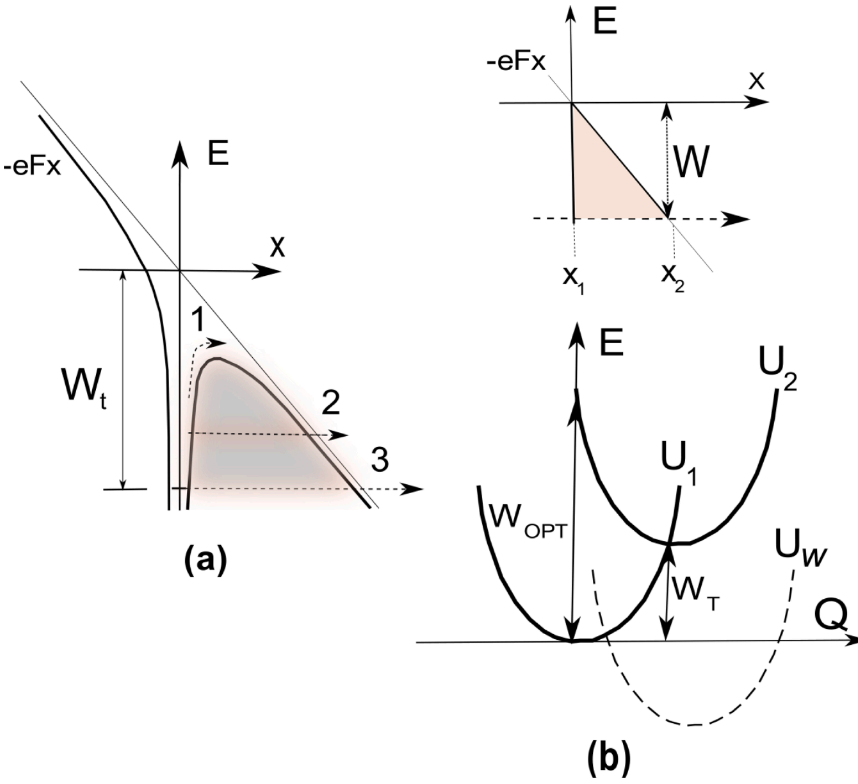


**Fig. 2.** Energy diagrams for two trap ionization mechanisms: (a) the Frenkel effect with TAT marked as: 1 - Frenkel effect, 2 - TAT, 3 – pure tunneling, $W_t$ - Coulomb trap energy, (b) multiphonon trap ionization mechanism; on top of the figure is the electron tunneling through a potential of zero radius (neutral trap); below are adiabatic terms: $U_1$ - potential energy of a trap filled with an electron, $U_2$ - potential energy of an empty trap, $U_W$ - potential energy of an empty trap in a strong electric field, $Q$ - configuration coordinate, $W_T$ and $W_{OPT}$ are the thermal and optical trap ionization energies, respectively.

Poisson equation. The equations for describing the charge transport in a-$SiN_x$ are as follows:

$$\frac{\partial n(x,t)}{\partial t} = \frac{1}{e}\frac{\partial j_n(x,t)}{\partial x} - \sigma^e \upsilon n(x,t)(N^e - n_t(x,t)) + n_t(x,t)P^e(x,t) - \sigma_r^e \upsilon n(x,t)p_t(x,t) \quad (1)$$

$$\frac{\partial n_t(x,t)}{\partial t} = \sigma^e \upsilon n(x,t)(N^e - n_t(x,t)) - n_t(x,t)P^e(x,t) - \sigma_r^h \upsilon p(x,t)n_t(x,t) \quad (2)$$

$$\frac{\partial p(x,t)}{\partial t} = \frac{1}{e}\frac{\partial j_p(x,t)}{\partial x} - \sigma^h \upsilon p(x,t)\left(N^h - p_t(x,t)\right) + p_t(x,t)P^h(x,t) - \sigma_r^h \upsilon p(x,t)n_t(x,t) \quad (3)$$

$$\frac{\partial p_t(x,t)}{\partial t} = \sigma^h \upsilon p(x,t)\left(N^h - p_t(x,t)\right) - p_t(x,t)P^h(x,t) - \sigma_r^e \upsilon n(x,t)p_t(x,t) \quad (4)$$

$$\frac{\partial F(x,t)}{\partial x} = -\frac{\partial^2 U(x,t)}{\partial x^2} = -e\frac{(n_t(x,t) + n(x,t) - p_t(x,t) - p(x,t))}{\varepsilon\varepsilon_0}, \quad (5)$$

where $n(x,t)$ and $n_t(x,t)$ are free and trapped electron concentrations, $p(x,t)$ and $p_t(x,t)$ are free and trapped hole concentrations, respectively, $P^{e,h}(x,t)$ is the ionization rate at a given electric field value ($F(x,t)$) and temperature ($T$), $U(x,t)$ is the electric potential, $N^{e,h}(x,t)$ is the trap concentration, $\sigma^{e,h}$ is the capture cross-section, $\sigma_r^{e,h}$is the recombination cross-section between free electrons with localized holes and free holes with localized electrons, $e$ is the electron charge, $\varepsilon = 7.5$ is the low-frequency dielectric constant of a-$SiN_x$ [4] and $\varepsilon_0$ is the electric constant. It was assumed that, at first, $n_t(x,0) = 0$ cm$^{-3}$ and $p_t(x,0) =$ 0 cm$^{-3}$, $n(x,0) = 0$ $cm^{-3}$ and $p(x,0) = 0$ cm$^{-3}$. As a boundary condition in a-$SiN_x$ for Eq. (5), the external voltage value $U$ applied to the structure is used; for Eqs. (1)–(4), $n(0, t) = j_n^{inj}/e\upsilon$, $p(d,t) = j_p^{inj}/e\upsilon$. Here, $j_n^{inj}$, $j_p^{inj}$ are the electron injection currents from the Si substrate and holes - from Al, respectively, which were calculated using the Fowler–Nordheim mechanism with the thermally assisted tunneling [30]. As the electric field, for the Fowler-Nordheim model, we took the field at the Si/a-$SiN_x$ interface and the Al/a-$SiN_x$ interface calculated on the basis of Poisson equation and used the same effective masses for electrons and holes as in the a-$SiN_x$ bulk [19]. The electron and hole currents density is related to the concentration of free electrons and holes by the following expressions $j_n(x) = en(x)\upsilon$ and $j_p(x) = -ep(x)\upsilon$, where we assumed that diffusion currents are negligible and both holes and electrons move with the same saturates drift velocity $\upsilon = 10^7$ cm/s, assumed independent of the field in the field region of interest, i.e. 2-7 MV/cm [31–33]. Carriers freely passed at the opposite ends of the $SiN_x$ sample: electrons - into the metal and holes - into the semiconductor. We did not consider the forces of the image based on the experimental results of [34]. The numerical solutions of Eqs. (1)–(5) are necessary to describe the a-$SiN_x$ polarization process after applying (changing) a voltage pulse. In some time ($\sim 10^{-3}$ s), after changing the voltage pulse, the electric current in the system becomes steady-state. The Poisson equation assumes that the traps $N^e(x,t)$ and $N^h(x,t)$ are initially neutral. This consideration is suitable for describing the charge transport using the multiphonon trap ionization mechanism. To describe the charge transport using the Frenkel model, we will assume that the $SiN_x$ bulk contains: $N^e(x,t)$ - positively charged traps for electrons and $N^h(x,t)$ - negatively charged traps for holes, and $N^e(x, t) = N^h(x,t)$. The electron capture onto electron traps leads to the appearance of an uncompensated negative charge from $N^h(x,t)$. Capturing a hole by hole traps leads to the appearance of an uncompensated positive charge from $N^e(x,t)$. This assumption makes it possible to use the system of Eqs. (1-5) when considering both the multiphonon trap ionization mechanism and the Frenkel effect with TAT. We did not

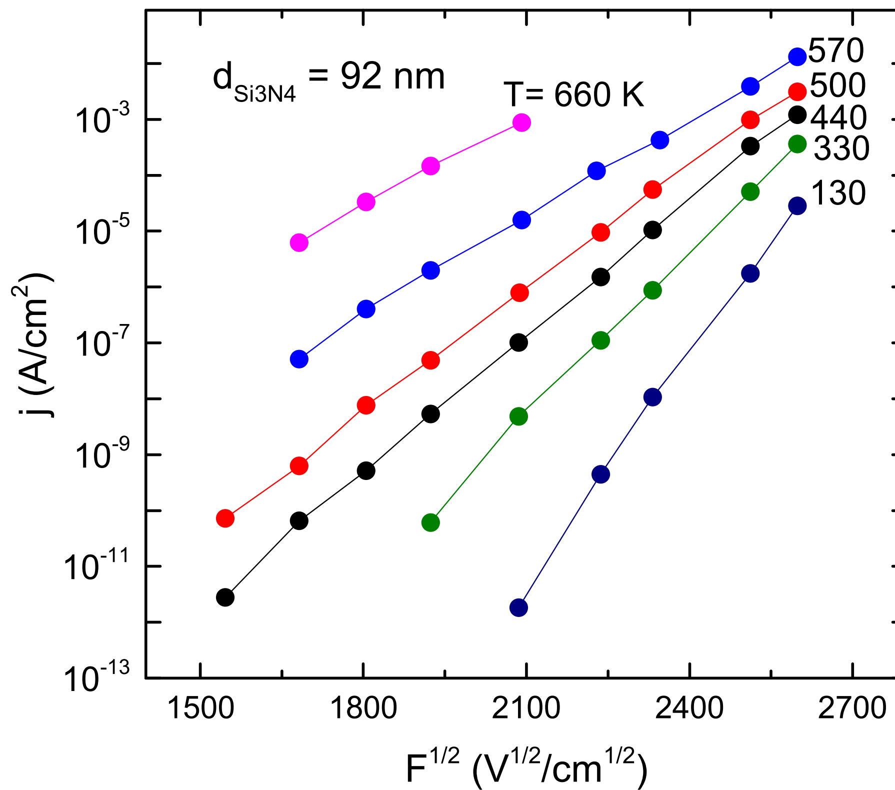


**Fig. 3.** Experimental I-V characteristics measured in a-$SiN_x$ (circles) at different temperatures (in Frenkel coordinates).

include $N^e(x,t)$, $N^h(x,t)$ in the Poisson equation in the form of $(N^h(x,t) - N^e(x,t))$ because this difference will always be zero.

To calculate the trap ionization probability, we used the Frenkel model, along with TAT, (Fig. 2(a)) and the multiphonon ionization mechanism (Fig. 2(b)). According to the Frenkel effect, the trap ionization probability is determined as in [22,23]:

$$P_F = \nu \exp\left(-\frac{W_t - \beta\sqrt{F}}{kT}\right); \quad \beta = \sqrt{\frac{e^3}{\pi\varepsilon_\infty\varepsilon_0}}. \tag{6}$$

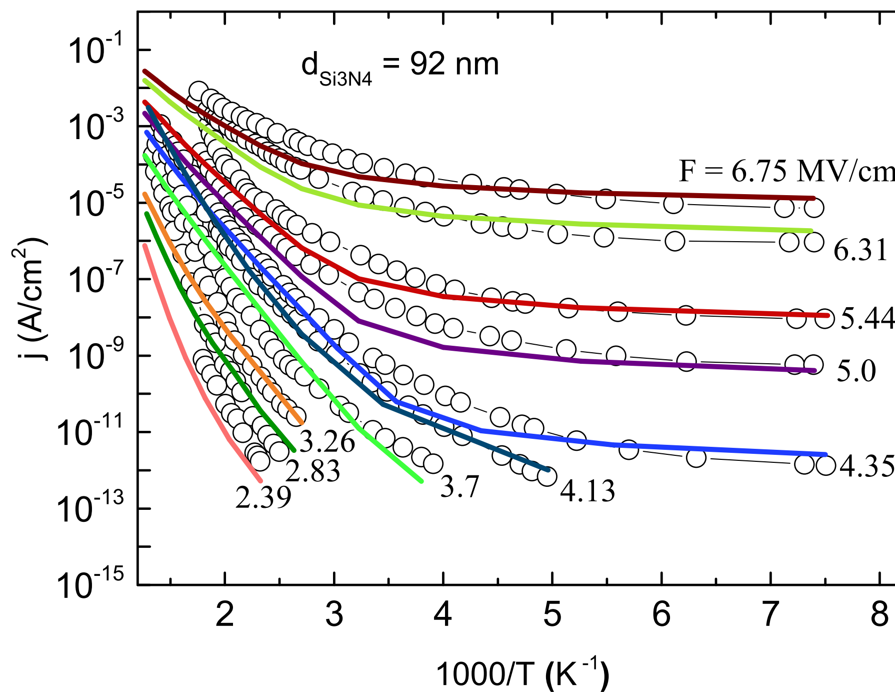


**Fig. 4.** The current *vs* temperature curves measured in a-$SiN_x$, as plotted in the Arrhenius coordinates for different applied external electric field values: circles – experiment and solid lines - calculation (Frenkel model with TAT). The following trap parameters were used in the calculations: $\nu = 10^9$ s$^{-1}$, $W_T^e = 1.5$ eV, $N^e = 8 \times 10^{18}$ cm$^{-3}$, $\sigma^e = 5 \times 10^{-13}$ cm$^2$, $\sigma_r^e = 5 \times 10^{-13}$ cm$^2$, $W_T^h = 1.5$ eV, $m_e^* = 3m_0$, $N^h = 8 \times 10^{18}$ cm$^{-3}$, $\sigma^h = 5 \times 10^{-13}$ cm$^2$, $\sigma_r^h = 5 \times 10^{-13}$ cm$^2$ and $m_h^* = 3m_0$.

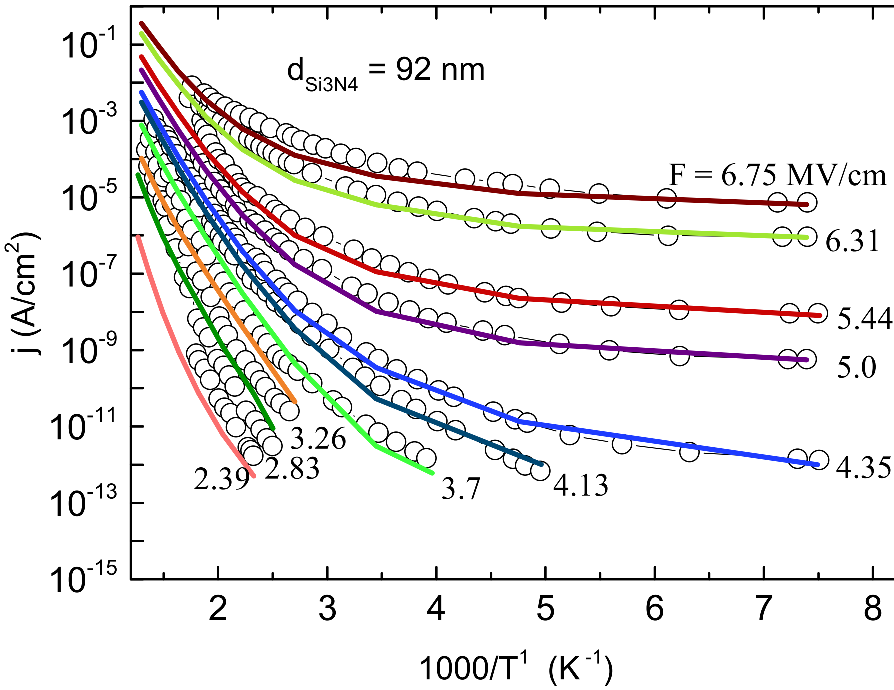


**Fig. 5.** The current *vs* temperature curves measured in a-SiN$_x$, as plotted in the Arrhenius coordinates for different applied external electric field values: circles – experiment and solid lines - calculation (multiphonon mechanism of trap ionization, exact model). The following trap parameters were used in the calculations: $W_T^e = 1.6$ eV, $W_{OPT}^e = 3.2$ eV, $W_{ph}^e = 0.064$ eV, $N^e = 6\times10^{18}$ cm$^{-3}$, $\sigma^e = 5\times10^{-14}$ cm$^2$, $\sigma_r^e = 5\times10^{-13}$ cm$^2$, $m_e^* = 0.6m_0$, $W_T^h = 1.6$ eV, $W_{OPT}^h = 3.2$ eV, $W_{ph}^h = 0.064$ eV, $N^h = 6\times10^{18}$ cm$^{-3}$, $\sigma^h = 5\times10^{-14}$ cm$^2$, $\sigma_r^h = 5\times10^{-13}$ cm$^2$ and $m_h^* = 0.6m_0$.

Here, $W_t$ is the trap energy, $\beta$is the Frenkel constant, $\varepsilon_\infty$=4.0 is the high-frequency dielectric constant [4], $k$ is the Boltzmann constant and $\nu$ is the frequency factor. In the original contributions by Frenkel, only the thermal ionization of Coulomb traps is considered. We expanded the Frenkel model [5], considered pure tunneling and TAT (Fig. 2(a)):

$$P_{TAT} = \frac{\nu}{kT}\int_0^{W_t-\beta\sqrt{F}} dW\exp\left(-\frac{W}{kT}-\frac{2}{\hbar}\int_{x_1}^{x_2}dx\sqrt{m^*(eV(x)-W)}\right), \qquad (7)$$

$$V(x) = W_t - \frac{e}{4\pi\varepsilon_\infty\varepsilon_0 x} - Fx.$$

Here, $W$ is the excited energy level, $m^*$ is the tunneling effective mass, values $x_1$, $x_2$ are classical turning points:

$$x_{1,2} = \frac{1}{2}\frac{W_t - W}{eF}\left(1 \pm \left(\frac{eF}{\pi\varepsilon\varepsilon_\infty(W_t-W)^2}\right)^{1/2}\right) \qquad (8)$$

The ionization rate by the Frenkel mechanism, along with TAT, was calculated with the formula:

$$P_{F,TAT} = P_F + P_{TAT} \qquad (9)$$

To calculate the trap ionization probability, the multiphonon ionization model is also used [26]. Within this model, the trap ionization probability is given by the expression:

$$P_{MF} = \sum_{n=-\infty}^{+\infty}\exp\left[\frac{nW_{ph}}{2kT} - S\coth\frac{W_{ph}}{2kT}\right]I_n\left(\frac{S}{\sinh(W_{ph}/2kT)}\right)P_i(W_T + nW_{ph}), \qquad (10)$$

$$P_i(W) = \frac{eF}{2\sqrt{2m^*W}}\exp\left(-\frac{4}{3}\frac{\sqrt{2m^*}}{heF}W^{3/2}\right), \quad S = \frac{W_{OPT}-W_T}{W_T},$$

where $W_T$ and $W_{OPT}$ are the thermal and optical trap ionization energies, respectively, $W_{ph}$ is the phonon energy and *In* is Bessel modified function.

## 3. Results and discussion

The experimental current-voltage (I–V) characteristics measured in a-SiN$_x$ at different temperatures (130 -660 K) in the Frenkel (lg(j)-$\sqrt{F}$) coordinates are shown in Fig. 3. As can be seen in the figure, in the lg(j)-$\sqrt{F}$ coordinates, the experimental I–V characteristics demonstrate a good straightening. As a rule, the I–V characteristic straightening, in the lg(j)-$\sqrt{F}$ coordinates, is considered as a sufficient basis for the applicability of Frenkel mechanism [22,35]. Our subsequent analysis shows that this approach is not correct.

The experimental current *vs* temperature curves (circles) measured in a-SiN$_x$, as plotted in the Arrhenius coordinates (lg(j)-T$^{-1}$), and their calculation (solid lines) using the Frenkel effect with TAT are shown in Fig. 4. All measurements were carried out at a positive potential at the Al electrode. It can be seen in the figure that the current value weakly depends on temperature at $T < 200$ K. The weak current dependence on temperature indicates the tunneling mechanism of trap ionization. An increase in temperature leads to a transition from the tunneling to TAT (Fig. (2a)).

The best agreement between the experiment and calculation was obtained for the following trap parameters: $\nu = 10^9$ s$^{-1}$, $W_t^e = 1.5$ eV, $m_e^* = 3m_0$ (where $m_0$ is a free electron mass), $N^e = 8\times10^{18}$ cm$^{-3}$, $\sigma^e = 5\times10^{-13}$ cm$^2$, $\sigma_r^e = 5\times10^{-13}$ cm$^2$, $W_t^h = 1.5$ eV, $m_h^* = 3m_0$, $N^h = 8\times10^{18}$ cm$^{-3}$, $\sigma^h = 5\times10^{-13}$ cm$^2$ and $\sigma_r^h = 5\times10^{-13}$ cm$^2$. In the original work by Frenkel [22], the frequency factor was estimated by the formula $\nu = W_t/h$ and in our case, it is $\nu \approx 10^{15}$ s$^{-1}$. The electron tunneling effective mass $m_{h,e} = 0.4m_0$ in a-SiN$_x$ was estimated in [30]. Thus, the Frenkel effect, with TAT taken into account, describes the experiments on the charge transport in a-SiN$_x$ in the entire range of electric fields and temperatures, while the frequency factor value used in the calculations is unphysically small. In addition, Frenkel theory predicts anomalously large tunneling effective mass values for electrons and holes, with TAT taken into account. An early small frequency factor value was obtained when describing the charge transport in the Frenkel model in a-SiN$_x$ [2, 30], BN [5], $Ta_2O_5$ [11].

The experimental current *vs* temperature curves (circles) measured in a-SiN$_x$, as plotted in the coordinates lg(j)-T$^{-1}$, and their calculation (solid lines) using the multiphonon ionization theory of traps [26] are

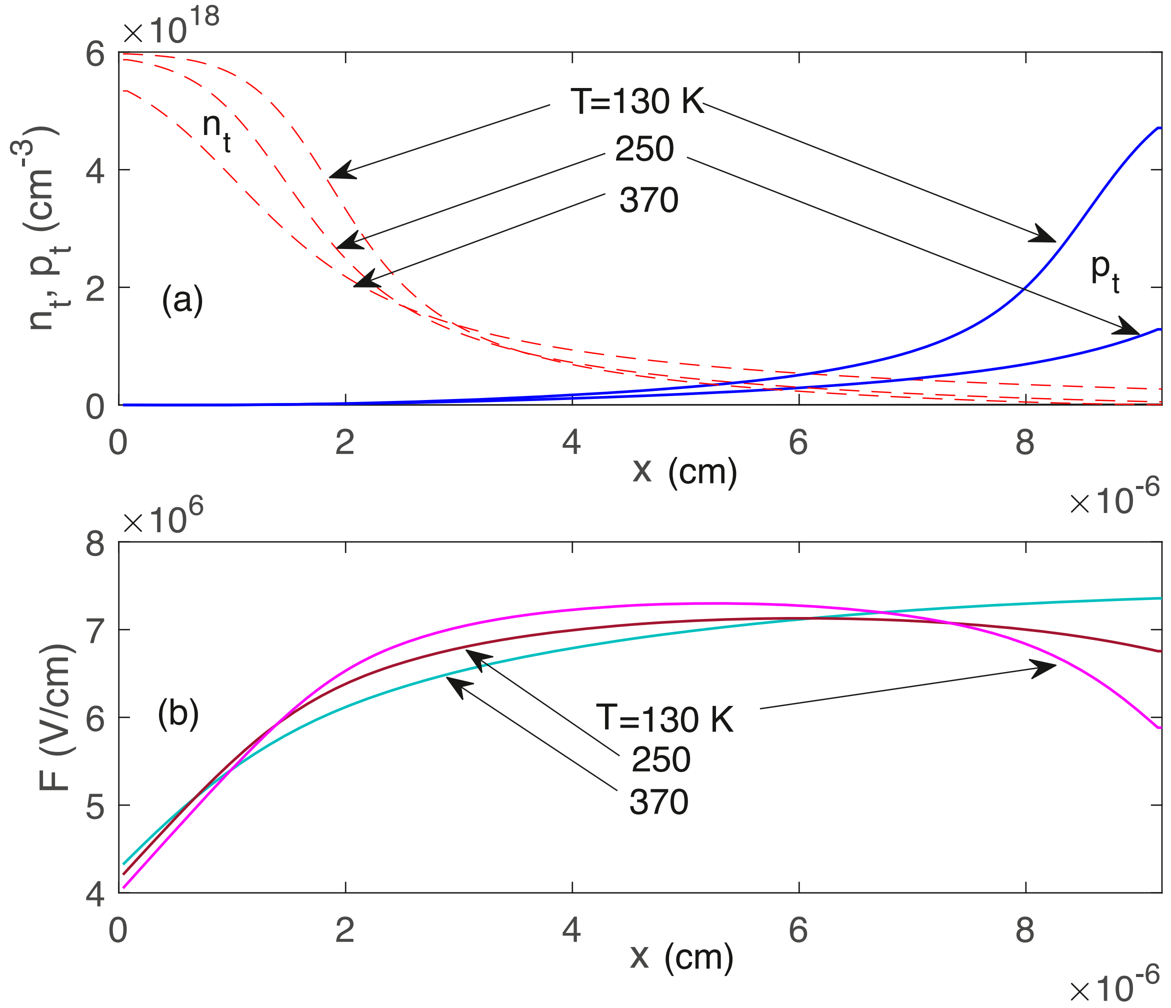


**Fig. 6.** Calculation in a-$SiN_x$ at a fixed potential (62 V) on Al for different temperatures: (a) the distribution of electrons and holes in the traps; (b) the electric field distribution. The following parameters were used in the calculations using the multiphonon trap ionization mechanism: $W_T^e = 1.6$ eV, $W_{OPT}^e = 3.2$ eV, $W_{ph}^e = 0.064$ eV, $N^e = 6 \times 10^{18}$ cm$^{-3}$, $\sigma^e = 5 \times 10^{-14}$ cm$^2$, $\sigma_r^e = 5 \times 10^{-13}$ cm$^2$, $m_e^* = 0.6m_0$, $W_T^h = 1.6$ eV, $W_{OPT}^h = 3.2$ eV, $W_{ph}^h = 0.064$ eV, $N^h = 6 \times 10^{18}$ cm$^{-3}$, $\sigma^h = 5 \times 10^{-14}$ cm$^2$, $\sigma_r^h = 5 \times 10^{-13}$ cm$^2$ and $m_h^* = 0.6m_0$.

shown in Fig. 5. The following trap parameters were used in the calculations: $W_T^e = 1.6$ eV, $W_{OPT}^e = 3.2$ eV, $W_{ph}^e = 0.064$ eV, $m_e^* = 0.6m_0$, $N^e = 6 \times 10^{18}$ cm$^{-3}$, $\sigma^e = 5 \times 10^{-14}$ cm$^2$, $\sigma_r^e = 5 \times 10^{-13}$ cm$^2$, $W_T^h = 1.6$ eV, $W_{OPT}^h = 3.2$ eV, $W_{ph}^h = 0.064$ eV, $m_h^* = 0.6m_0$, $N^h = 6 \times 10^{18}$ cm$^{-3}$, $\sigma^h = 5 \times 10^{-14}$ cm$^2$ and $\sigma_r^h = 5 \times 10^{-13}$ cm$^2$. The calculation gives a satisfactory agreement with the experiment for the entire range of electric fields and temperatures (Fig. 5).

The calculation shows that, in weak electric fields (~ 2.4 - 3 MV/cm), the captured charge with a concentration of ~ $10^{15}$ cm$^{-3}$ is distributed uniformly over the a-$SiN_x$ thickness at all temperatures.

The electric field created by the charge with such a low concentration, practically, does not change (does not screen) the external field. The electric field remains constant throughout the a-$SiN_x$ sample. For this reason, for a given external electric field, the trap ionization probability is the same in the entire a-$SiN_x$ sample and changes only due to a change in temperature. In the high electric field region, over the entire temperature range, the carriers injected into a-$SiN_x$ are captured mainly near the contacts (Fig. 6(a)). With decreasing the temperature, the trap ionization probability is decreased. This leads to an increase in the trapped carriers concentration near the contacts and to an increase in the external electric field screening, and, as a consequence, to a decrease in the Fowler-Nordheim current. The changes of the electric field distribution in a-$SiN_x$, depending on temperature, are shown in Fig. 6(b). It can be seen in the figure that the electric field is inhomogeneous near the Si/a-$SiN_x$ interface, where it varies in the range from 4.0 to 7.5 MV/cm.

For high electric fields, an approximate formula is proposed for calculating the trap ionization probability [27,28]:

$$P = \frac{F}{2\sqrt{2m * W_{OPT}}} \exp\left( -\frac{4}{3}\frac{\sqrt{2m^*}}{\hbar F} W_{OPT}^{3/2} + 4b\frac{m^*\omega}{\hbar}\frac{W_{OPT}^2}{F^2} cth\left(\frac{\hbar\omega}{2kT}\right)\right);$$
$$b = \frac{4(W_{OPT} - W_T)}{W_{OPT}}; \quad \omega = \frac{W_{ph}}{\hbar}. \tag{11}$$

This theory is valid for electric fields over $F_{min}$ [28]:

$$F_{\min} = \frac{\omega\sqrt{2m * W_{OPT}}}{e}, \tag{12}$$

where $\omega$ is the trap "core" vibration frequency which can be estimated from the expression $\omega \approx W_{ph}/\hbar$. The estimate yields $F_{min} = 4.3$ MV/cm. The calculation for this model is shown in Fig. 7. The following parameters were used in the calculations: $W_T^e = 1.65$ eV, $W_{OPT}^e = 3.3$ eV, $W_{ph}^e = 0.05$ eV, $m_e^* = 0.6m_0$, $N^e = 6 \times 10^{18}$ cm$^{-3}$, $\sigma^e = 5 \times 10^{-14}$ cm$^2$, $\sigma_r^e = 5 \times 10^{-13}$ cm$^2$, $W_T^h = 1.65$ eV, $W_{OPT}^h = 3.3$ eV, $W_{ph}^h = 0.05$ eV, $m_h^* = 0.6m_0$, $N^h = 6 \times 10^{18}$ cm$^{-3}$, $\sigma^h = 5 \times 10^{-14}$ cm$^2$ and $\sigma_r^h = 5 \times 10^{-13}$ cm$^2$. The calculation demonstrates a good agreement with the experiment for

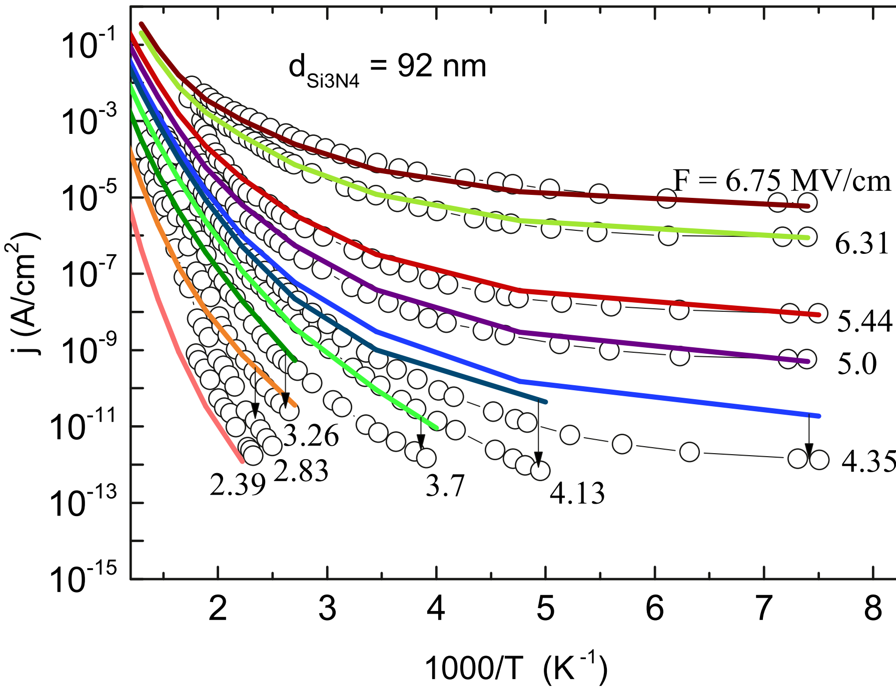


**Fig. 7.** The current *vs* temperature curves measured in a-$SiN_x$, as plotted in the Arrhenius coordinates for different applied external electric field values: circles – experiment and solid lines - calculation (approximate multiphonon trap ionization model). The following trap parameters were used in the calculations: $W_T^e = 1.65$ eV, $W_{OPT}^e = 3.3$ eV, $W_{ph}^e = 0.05$ eV, $m_e^* = 0.6m_0$, $N^e = 6 \times 10^{18}$ cm$^{-3}$, $\sigma^e = 5 \times 10^{-14}$ cm$^2$, $\sigma_r^e = 5 \times 10^{-13}$ cm$^2$, $W_T^h = 1.65$ eV, $W_{OPT}^h = 3.3$ eV, $W_{ph}^h = 0.05$ eV, $N^h = 6 \times 10^{18}$ cm$^{-3}$, $\sigma^h = 5 \times 10^{-14}$ cm$^2$, $\sigma_r^h = 5 \times 10^{-13}$ cm$^2$ and $m_h^* = 0.6m_0$. The arrows indicate the correspondences between the calculated and experimental curves.

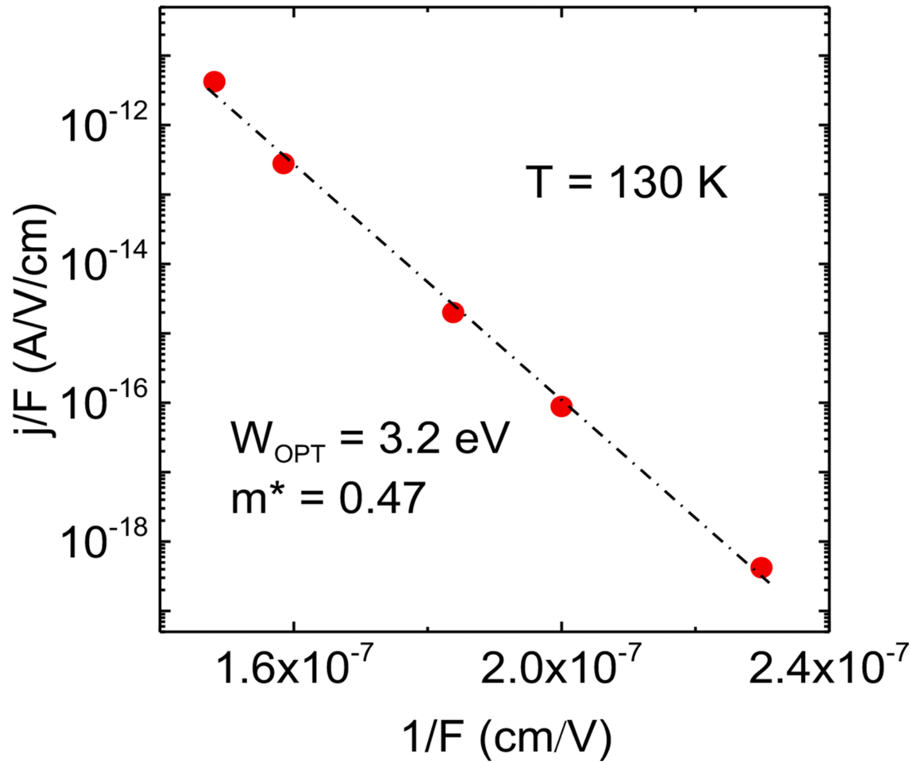


**Fig. 8.** I-V characteristics measured in a-$SiN_x$ at 130 K in j/F-1/F coordinates.

electric fields above 5 MV/cm. At lower electric fields, a discrepancy between the experiment and calculation is observed.

At low temperatures (130 K) in high electric fields, the main trap ionization mechanism is the direct carrier tunneling through a triangular barrier with the $W_{OPT}$ energy without phonon participation [27, 28] (Fig. 2(b)). In this case, the ionization probability in the presence of an electric field is given by the expression:

$$P = \frac{eF}{2\sqrt{2m^* W_{OPT}}} \exp\left(-\frac{4}{3}\frac{\sqrt{2m*}}{\hbar eF} W_{OPT}{}^{3/2}\right). \quad (13)$$

In Fig. 8, for temperature $T = 130$ K and electric fields more than $4.3 \times 10^6$ V/cm, an experimental current-voltage characteristic is plotted in the coordinates lg(j/F)-1/F. From the slope of the obtained dependence (Fig. 8), for the high electric field region, the electron tunneling effective mass was estimated for the optical energy of the trap

$W_{OPT} = 3.2$ eV, which was $m^* = 0.47m_0$.

The value $m^* = 0.47m_0$ estimated from the slope of the lg(j/F)-1/F dependence (Fig. 8) turned out to be less than the mass $m_e = 0.6m_0$ obtained in the experimental simulation, taking into account the formulas (1-5). Such a discrepancy can be attributed to the fact that, when assessing the trap ionization probability in the first case, the mean field ($F = V/d$) was used, and, in the second one, the local (coordinate-dependent) electric field obtained by solving the Poisson equation, taking into account the captured charge inhomogeneity in the a-$SiN_x$ bulk.

There arises a question as for why, when using the Frenkel effect together with TAT, it is necessary to use a small frequency factor and an anomalously large tunneling effective mass in the calculations, but not in the case of the multiphonon ionization mechanism. The main reason lies in the fact that an electron in the multiphonon mechanism tunnels through a barrier, which, depending on the electric field and temperature, varies in the range from 0 to $W_{OPT}$. In high electric fields, an electron tunnels through a barrier with an energy $W_{OPT}$ (formula 11), i.e. with an energy of ~ 3.2 eV. A similar effect was observed in $SiO_2$ [36], where it was shown that the electron trap has an energy of ~ 3.0 eV. At the same time, when using the Frenkel effect, along with TAT, the energy $W_t$, which is ~ 1.5 eV, is used in the calculations. The same speculations are applicable for trapped holes.

The multiphonon trap ionization model in a-$SiN_x$ assumes a strong polaron effect (a large difference between thermal and optical ionization energies). Earlier, the polaron model of electron and hole traps in a-$SiN_x$ was discussed in [37,38]. According to this model, the capture of electrons and holes in a-$SiN_x$ is carried out onto the minimum silicon cluster (Si-Si bond). The polaron model assumes that the Si-Si bond, or a silicon cluster consisting of several silicon atoms, is a deep trap for electrons, a deep trap for holes and a recombination center. The quantum-chemical modeling of the Si-Si bond in a-$SiN_x$ qualitatively confirms this hypothesis [39–41].

## 4. Conclusion

In this work, the charge transport mechanism in amorphous a-$SiN_x$ was studied experimentally and theoretically. The experimental results (the current dependence on the temperature at different electric field values) were compared with the calculations. The model based on the Frenkel effect, along with TAT, formally describes the experimental results, but, in this case, it is necessary to use an anomalously large tunneling effective mass and an unphysically small frequency factor. The multiphonon trap ionization mechanism satisfactorily describes the experimental results for acceptable physical parameters. The simplified model [28] based on the multiphonon trap ionization mechanism for high electric fields also describes the experimental results for electric fields above 4.3 MV/cm. One and the same parameters were obtained for electron and hole traps. Our analysis indicates that the trap spectrum in a-$SiN_x$ is discrete. For a quantitative description of charge transport, there is no need to introduce the concept of an energy-continuous trap spectrum (Eq. 10).

## CRediT authorship contribution statement

**Yu.N. Novikov:** Conceptualization, Data curation, Writing – original draft, Writing – review & editing. **V.A. Gritsenko:** Conceptualization, Data curation, Writing – original draft, Writing – review & editing.

## Declaration of Competing Interest

The authors declare that they have no known competing financial interests or personal relationships that could have appeared to influence the work reported in this paper.

## Acknowledgments

Experiments were carried out under the grant of the Russian Foundation for Basic Research (RFBR) (project № 19-29-03018) and, partially, the work was carried out under state contract with the ISP SBRAS program № 0242-2021-0003 (models and numerical calculations).

## References

[1] D.S. Jeong, C.S. Hwang, Tunneling current from a metal electrode to many traps in an insulator, Phys. Rev. B 71 (2005), 165327, https://doi.org/10.1103/PhysRevB.71.165327.
[2] S.P. Lau, J.M. Shannon, B.J. Sealy, Changes in the Poole–Frenkel coefficient with current induced defect band conductivity of hydrogenated amorphous silicon nitride, J. Non-Cryst. Solids 277–230 (1998) 533–537, https://doi.org/10.1016/S0022-3093(98)00113-6.
[3] H. Bachhofer, H. Reisinger, E. Bertagnolli, H. von Philipsborn, Transient conduction in multidielectric silicon–oxide–nitride–oxide semiconductor structures, J. Appl. Phys. 89 (2001) 2791–2800, https://doi.org/10.1063/1.1343892.
[4] S. Manzini, Electronic processes in silicon nitride, J. Appl. Phys. 62 (1987) 3278–3284, https://doi.org/10.1063/1.339334.
[5] Yu.N. Novikov, V.A. Gritsenko, The charge transport mechanism in amorphous boron nitride, J. Non-Cryst. Solids 544 (2020), 120213, https://doi.org/10.1016/j.jnoncrysol.2020.120213.
[6] Yu.N. Novikov, V.A. Gritsenko, K.A. Nasyrov, Charge transport mechanism in amorphous alumina, Appl. Phys. Lett. 94 (2009), 222904, https://doi.org/10.1063/1.3151861.
[7] G. Jegert, A. Kersch, W. Weinreich, U. Schroder, P. Lugli, Modeling of leakage currents in high-κ dielectrics: Three-dimensional approach via kinetic Monte Carlo, Appl. Phys. Lett. 96 (2010), 062113, https://doi.org/10.1063/1.3310065.
[8] D.R. Islamov, V.A. Gritsenko, T.V. Perevalov, V.S. Aliev, V.A Nadolinny, A. Chin, Oxygen Vacancies in Zirconium Oxide as the Blue Luminescence Centres and Traps Responsible for Charge Transport: Part II – Films, Materialia 15 (2021), 100980, https://doi.org/10.1016/j.mtla.2020.100980.
[9] E. Atanassova, A. Paskaleva, N. Novkovski, M. Georgieva, Conduction mechanisms and reliability of thermal $Ta_2O_5$-Si structures and the effect of the gate electrode, J. Appl. Phys. 97 (2005), 094104, https://doi.org/10.1063/1.1884758.
[10] K.V. Egorov, D.S. Kuzmichev, P.S. Chizhov, Y.Y. Lebedinskii, C.S. Hwang, A. M. Markeev, Situ Control of Oxygen Vacancies in TaOx Thin Films via Plasma-Enhanced Atomic Layer Deposition for Resistive Switching Memory Applications, ACS Appl. Mater. Interfaces 9 (2017) 13286–13292, https://doi.org/10.1021/acsami.7b00778.
[11] V.A. Gritsenko, T.V. Perevalov, V.A. Voronkovskii, A.A. Gismatulin, V. N. Kruchinin, V.S. Aliev, V.A. Pustovarov, I.P. Prosvirin, Y. Roizin, Charge Transport and the Nature of Traps in Oxygen Deficient Tantalum Oxide, ACS Appl. Mater. Interfaces 10 (2018) 3769–3775, https://doi.org/10.1021/acsami.7b16753.
[12] A.V. Shaposhnikov, T.V. Perevalov, V.A. Gritsenko, C.H. Cheng, A. Chin, Mechanism of $GeO_2$ resistive switching based on the multi-phonon assisted tunneling between traps, Appl. Phys. Lett. 100 (2012), 243506, https://doi.org/10.1063/1.4729589.
[13] D.R. Islamov, V.A. Gritsenko, C.H. Cheng, A. Chin, Origin of traps and charge transport mechanism in hafnia, Appl. Phys. Lett. 105 (2014), 222901, https://doi.org/10.1063/1.4903169.
[14] A.A. Gismatulin, V.A. Gritsenko, D.S. Seregin, K.A. Vorotilov, M.R. Baklanov, Charge transport mechanism in periodic mesoporous organosilica low-k dielectric, Appl. Phys. Lett. 115 (2019), 082904, https://doi.org/10.1063/1.5113633.
[15] V.-V. Le, T.-T. Nguyen, K.-H. Pham, The structural correlation and mechanical properties in amorphous silicon nitride under densification, J. Non-Cryst. Solids 363 (2013) 6–12, https://doi.org/10.1016/j.jnoncrysol.2012.12.011.
[16] C.H. Hsu, Y.P. Lin, H.J. Hsu, C.C. Tsai, Enhanced spectral response by silicon nitride index matching layer in amorphous silicon thin-film solar cells, J. Non-Cryst. Solids 358 (2012) 2324–2326, https://doi.org/10.1016/j.jnoncrysol.2011.12.102.
[17] V.A. Gritsenko, Silicon Nitride on Si: Electronic Structure for Flash Memory Devices, World Scientific (2016), https://doi.org/10.1142/9789814740487_0006.
[18] Y.(Larr) Yang, M.H. White, Charg e retention of scaled SONOS nonvolatile memory devices at elevated temperatures, Solid-State Electron 44 (2000) 949–958, https://doi.org/10.1016/S0038-1101(00)00012-5.
[19] Y. Wang, M.H. White, An analytical retention model for SONOS nonvolatile memory devices in the excess electron state, Solid-State Electron 49 (2005) 97–107, https://doi.org/10.1016/j.sse.2004.06.009.
[20] A. Suhane, A. Arreghini, R. Degraeve, G. Van den bosch, L. Breuil, M.B. Zahid, M. Jurczak, K. De Meyer, J. Van Houdt, Validation of Retention Modeling as a Trap-Profiling Technique for SiN-Based Charge-Trapping Memories, IEEE Electron. Device Lett. 31 (2010) 77–79, https://doi.org/10.1109/LED.2009.2035718.
[21] A. Padovani, L. Larcher, V.D. Marca, P. Pavan, H. Park, G. Bersuker, Charge trapping in alumina and its impact on the operation of metal-alumina-nitride-oxide-silicon memories: Experiments and simulations, J. Appl. Phys. 110 (2011), 014505, https://doi.org/10.1063/1.3602999.

[22] Y.I. Frenkel, On the theory of electrical breakdown in dielectrics and electronic semiconductors, J. Exp. Theor. Phys 8 (1938) 1292.
[23] J. Frenkel, On Pre-Breakdown Phenomena in Insulators and Electronic Semi-Conductors, Phys. Rev. B 54 (1938) 647–648, https://doi.org/10.1103/PhysRev.54.647.
[24] R. Audino, F. Cannistraci, G. Morello, P. Valenti, PECVD a-SiNx:H films for dielectric insulation in buried ridge structure Fabry-Perot and distributed feedback laser devices, J. Non-Cryst. Solids 187 (1995) 477–483, https://doi.org/10.1016/0022-3093(95)00180-8.
[25] S.M. Sze, Current Transport and Maximum Dielectric Strength of Silicon Nitride Films, J. Appl. Phys. 18 (1967) 2951–2956, https://doi.org/10.1063/1.1710030.
[26] S.S. Makram-Ebeid, M. Lannoo, Quantum model for phonon-assisted tunnel ionization of deep levels in a semiconductor, Phys Rev. B 25 (1982) 6406–6424, https://doi.org/10.1103/PhysRevB.25.6406.
[27] V.N. Abakumov, V.I. Perel, I.N. Yassievich, Nonradiative Recombination in Semiconductors, Elsevier, North Holland, 1991.
[28] V. Karpus, Effect of electron-phonon interaction on the ionization of deep centers by a strong electric field, JETF Letter 44 (1986) 430.
[29] Yu.N. Novikov, Charge transport in $HfO_2$ due to multiphonon traps ionization mechanism in $SiO_2/HfO_2$ stacks, J. Appl. Phys. 113 (2013), 024109, https://doi.org/10.1063/1.4775407.
[30] V.A. Gritsenko, E.E. Meerson, Yu.N. Morokov, Thermally assisted hole tunneling at the $Au-Si_3N_4$ interface and the energy-band diagram of metal-nitride-oxide-semiconductor structures, Phys. Rev. B 57 (1998) R2081–R2083, https://doi.org/10.1103/PhysRevB.57.R2081.
[31] P.C. Arnett, Transient conduction in insulators at high fields, Journal of Applied Physics 46 (1975) 5236–5243, https://doi.org/10.1063/1.321592.
[32] C.M. Svensson, The conduction mechanism in silicon nitride films, J. App. Phys. 48 (1977) 329, https://doi.org/10.1063/1.323382.
[33] R.C. Hughes, Charge-Carrier Transport Phenomena in Amorphous SiO: Direct Measurement of the Drift Mobility and Lifetimes, Phys. Rev. Lett. 30 (1973) 1333–1336, https://doi.org/10.1103/PhysRevLett.30.1333.
[34] Z.A. Weinberg, A. Hartstein, Photon assisted tunneling from aluminum into silicon dioxide, Solid State Commun 20 (1976) 179–182, https://doi.org/10.1016/0038-1098(76)90170-8.
[35] Y.-C. Jeon, H.-Y. Lee, S.-K. Joo, I-V characteristics of electron-cyclotron-resonance plasma-efihanced chemical-vapor-deposition silicon nitride thin films, J. Appl. Phys. 75 (1993) 979–984, https://doi.org/10.1063/1.356455.
[36] K. Yamabe, Y. Miura, Discharge of trapped electrons from MOS structures, J. Appl. Phys. 51 (1980) 6258–6264, https://doi.org/10.1063/1.327612.
[37] V.A. Gritsenko, P.A. Pundur, Multiphonon capture and radiative transitions in $\alpha$-$Si_3N_4$, Sov. Physics of the solid state 28 (1986) 3239.
[38] P.A. Pundur, J.G. Shvalgin, V.A. Gritsenko, On the Nature of Deep Centers Responsible for the Memory Effect and Luminescence of a-$SiN_x$ with $x<4/3$, Phys. Stat. Sol. 94 (1986) k701, https://doi.org/10.1002/pssa.2210940261. -k112.
[39] V.A. Gritsenko, H. Wong, J.B. Xu, R.M. Kwok, I.P. Petrenko, B.A. Zaitsev Yu. N. Morokov, N Yu, Novikov Excess silicon at the silicon nitride/thermal oxide interface in oxide–nitride–oxide structures, J. Appl. Phys. 86 (1999) 3234–3240, https://doi.org/10.1063/1.371195.
[40] M. Petersen, Y. Roizin, Density functional theory study of deep traps in silicon nitride memories, Appl. Phys. Lett. 89 (2006), 053511, https://doi.org/10.1063/1.2260829.
[41] M.-E. Grillo, S.D. Elliott, Native defects in hexagonal $\beta$-$Si_3N_4$ studied using density functional theory calculations, Phys. Rev. B 83 (2011), 085208, https://doi.org/10.1103/PhysRevB.83.085208.